5

Microporous Honeycomb-Structured Polymer Films

L.V. Govor
Institute of Physics, University of Oldenburg, D-26111 Oldenburg, Germany
leonid.govor@uni-oldenburg.de

5.1. INTRODUCTION

Micrometre-sized porous membranes with highly ordered honeycomb structures are technologically important for a variety of applications. They are of interest for use in chemistry and life science [1]. As a consequence of their strong periodicity, these membranes made from diverse compounds possess the characteristic properties of polymer photonic crystals [2–4]. For the manufacturing of such membranes, a large variety of the methods exists [5]. Self-organization may offer some advantages in this field: the patterning process can function in different media, and cost-intensive large-scale technology is not necessary. By self-organized processes, one is able to develop distinct structures with a regular geometrical configuration (e.g., networks with hexagonal cells). Nowadays, the ordered mesoporous solids with nanoscale pore sizes are fabricated by self-organization of spherical micelles from a diblock copolymer system in a selective solvent [6]. The mesoporous materials can be formed by colloidal templating [7,8]; colloidal crystals of polystyrene or silica spheres are composed of fluid that fills the space between the spheres. Thereafter, the templating spheres are removed to result in the creation of a porous solid where the dimension of the pores matches those of the templating spheres.

Water-assisted formation of ordered mesoporous membranes was described in the numerous articles [9–14]. In this case, the ordered membranes are formed by the condensation of water vapour on the fluid polymer solution film and by a subsequent evaporation of a solvent from the polymer solution. Recently, we have developed a preparation method that allows the membrane formation with evenly shaped hexagonal cells with a diameter

of about 1–2 μm [15–17]. In the above works, we have described in detail the technology how to get mesoporous membranes from different polymers. Simultaneously, some effort has been undertaken to interpret the self-organizing mechanism of patterning by thermodynamic processes that take place between water droplets on the fluid polymer solution surface. We have suggested that the stabilization of water droplets on a fluid surface is indispensable for ordered structure formation. In the following, the most important stabilization parameters are discussed that can influence the growth of condensing water droplets on the fluid polymer solution layer and their interaction between each other.

5.2. EXPERIMENTAL FORMATION OF POLYMER HONEYCOMB STRUCTURES

For the formation of a self-organized honeycomb polymer network, we have developed a four-step method. Figure 5.1 shows these steps: (a) deposition of one drop of polymer solution (liquid F1) on the cooled water surface (liquid F2, 3–5 °C); (b) spreading of one drop of polymer solution to an extremely thin layer; (c) interaction of water vapour (air with 100%, 75%, 32% or 19% relative humidity at 20 °C) with the polymer thin film surface for structuring/self-organization of the lateral water droplets distribution and polymer network formation and (d) mechanical removal of the structured network from the liquid and potential fixation by annealing.

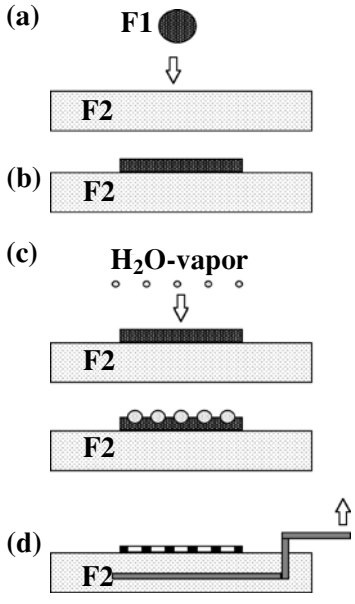

FIGURE 5.1. Formation of a self-organized honeycomb polymer structure: (a) deposition of one drop of polymer solution F1 on the cooled water surface F2; (b) spreading of one drop of polymer solution to a thin layer; (c) water vapour condensing on the polymer film surface; growing of water droplets and building of the compact hexagonal structure, i.e., polymer network and (d) drying of the polymer network and transfer from the water surface to a fixed substrate.

The condition for the spreading of a drop of liquid F1 on the surface of liquid F2, is given by thermodynamic arguments [18]

$$\sigma_{F2/G} > \sigma_{F1/G} + \sigma_{F1/F2} \tag{5.1}$$

where $\sigma_{F1/F2}$, $\sigma_{F1/G}$ and $\sigma_{F2/G}$ denote the surface tension between the liquids F1 and F2, between liquid F1 and gas G (G is air) and between liquid F2 and gas G, respectively. The degree of spreading of a film of liquid F1 over liquid F2 is characterized by the spreading coefficient which is determined as [18]

$$S_{F1/F2} = \sigma_{F2/G} - \sigma_{F1/G} - \sigma_{F1/F2}. \tag{5.2}$$

For $S_{F1/F2} > 0$, the total spreading is achieved, i.e., the liquid drop F1 will cover the whole surface of the liquid F2 and, thereby, forms a monomolecular layer at the edge. For $S_{F1/F2} < 0$, there is no spreading.

5.2.1. Formation of Nitrocellulose Networks

The coating of one drop of the 1% nitrocellulose solution in amyl acetate on the cooled water surface leads to a complete spreading along that surface [16]. The surface tension coefficient of the 1% nitrocellulose solution in amyl acetate has a value $\sigma_{F1/G}$ (20 °C) = 24.6 mN/m. Distilled water which was cooled down to 3–5 °C possesses a surface tension coefficient of $\sigma_{F2/G} = 74.9$ mN/m. For the surface tension of the 1% nitrocellulose solution in amyl acetate on water, we take the value $\sigma_{F1/F2} = 12$ mN/m. The demand for the total spreading of one drop of the 1% nitrocellulose solution in amyl acetate on the cooled water surface is fulfilled because we have $S_{F1/F2} = 38.3$ mN/m.

The size of the spread thin polymer layer in the vessel (with a diameter of 93 mm) was 70 mm. Since the volume of the spread drop was 0.015 cm^3, the thickness of the resulting spread liquid polymer layer can be estimated to 3.9 μm. Our thin film was subject to the influence of water vapour which induces the self-organized formation of a honeycomb network structure. There was no control of the size of the water droplets, but there was control of the relative humidity of air which was about 75% at a temperature of 20 °C. Depending on the time elapsed after the water vapour has begun to affect the polymer film, one obtains a variety of network distinguished both in form and size. During our experiments, the above time span changed between 1 second and 60 seconds. In the final step, after having dried the network, it was transferred from the surface of water to a sapphire substrate.

5.2.2. Formation of Poly(p-Phenylenevinylene) and of Poly(3-Octylthiophene) Networks

For the formation of a self-organized honeycomb poly(*p*-phenylenevinylene) (PPV) and poly(3-octylthiophene) (P3OT) networks, we have used (a) a 2% xylene solution of the PPV precursor with $\sigma_{F1/G}$(20 °C) = 30 mN/m and (b) a 2% xylene solution of polythiophene with a nearly equivalent value of the surface tension. The surface tension between both 2% polymers solution in xylene and water (liquid F2) amounts to $\sigma_{F1/F2}$(20 °C) = 36.1 mN/m. From Equation (5.2), we can calculate the spreading coefficient that is about $S_{F1/F2} = 8.8$ mN/m, i.e., the condition (1) is fulfilled.

The thin polymer solution film formed on the surface of liquid water was then (immediately after spreading) subjected to water vapour (air with 19% relative humidity at a temperature of 20 °C). After the self-organization process of the water droplets on the polymer film has taken place, the polymer film builds up a honeycomb structure. It should be noted that the diameter of the initial spread liquid polymer layer in the vessel (with a diameter of 93 mm) at the beginning was about 50 mm. Then the size of liquid polymer layer decreases to about 20–30 mm. The thickness of the resulting dry polymer layer was not homogeneous. The edge of the polymer layer was thinner and in this area the formation of hexagonal network occurs. The middle area of the layer was thicker and not structured. After having dried the network, it was transferred from the surface of water to a substrate (quartz, glass or indium–tin–oxide-plated glass).

5.3. SELF-ASSEMBLED NETWORKS OF POLYMERS

5.3.1. Nitrocellulose Networks

In the following, we will consider the network structures, obtained by the procedure described in Section 5.2. Having brought the water vapour on the polymer layer and having dried the polymer layer with a diameter of 70 mm, a fractal-like geometry occurred, i.e., areas (stripes) with network structures and areas without them are found. The majority of the structured stripes was distributed at the edge of the polymer layer and had normally the width of 0.5 mm and the length of 20 mm. The stripes can be connected with or separated from each other. Figure 5.2a shows a scanning electron microscope (SEM) picture of hexagonal nitrocellulose cells as a fragment. In this case, the water vapour was coated 10 seconds after spreading the polymer layer onto the cooled water surface. Note the strong homogeneity and reproducibility of the individual cells inside the network structure. For a more detailed look at the geometry, the picture of only a few cells is displayed in Figure 5.2b. The interpore distance amounts to 2.6 μm and the width of the walls to about 0.4 μm. The cross section of the pore wall perpendicular to the photograph plane offers the shape of a T-section. The latter means that each hexagonal cell lies on a hexagonal base also having extremely thin side walls. The height of the base is 0.5 μm. Each one of these six side walls represents some kind of a frame with various thicknesses along the circuit on which a thin polymer film is stretched. In most cases, the polymer film unveils an oval aperture in the middle of the frame.

Few structured big stripes have a different interpore distance on the edge (for example, 2 μm) and at the centre (for example, 6 μm) of the stripe. Figure 5.3 shows a SEM image of different fragments of one structured stripe after the annealing for 1 hour at a temperature of 950 °C under vacuum conditions. Figure 5.3a shows the network fragment between the edge and the centre of the stripe. It can be seen that the cross section of the pore wall perpendicular to the photograph plane for a cell with the diameter about 2–4 μm does not represent the shape of a T-section, i.e., the pore wall merges together after annealing. As a result, we observe two-dimensional cells. Figure 5.3b shows the network fragment at the centre of stripe after annealing. A three-dimensional cell from a carbon network pattern obtained from a corresponding nitrocellulose structure after

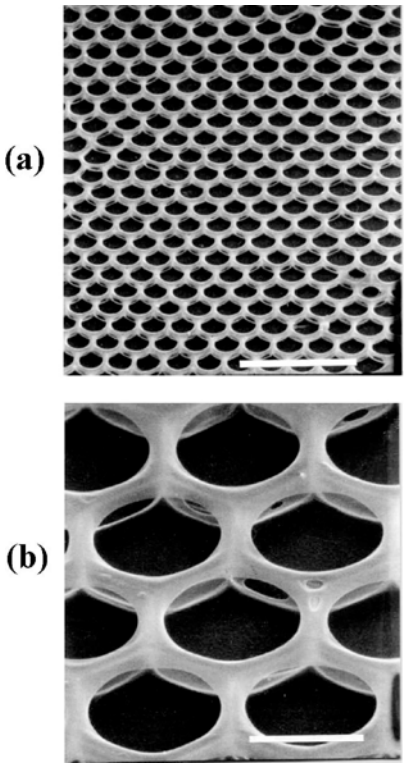

FIGURE 5.2. SEM images of a nitrocellulose network which were prepared via coating the water vapour 10 seconds after having spread the polymer layer onto the cooled water surface. Scale bars: (a) 10 μm and (b) 2 μm.

annealing is shown in Figure 5.3b. Regions of such structural form extend over an area of about (30 × 30) μm^2. Note that such kind of network patterning was only observed in the case where the cells have a relatively large diameter. It is obvious that the upper and lower hexagonal cells (one placed on the top of the other)—both with a diameter of 6 μm—are practically equal. The two cells are connected only at the corners. The height of the connection is approximately 1.5 μm. The diameter of the pore wall amounts to approximately 0.25 μm.

Figure 5.4a gives another SEM images of a nitrocellulose network with a different kind of structure (in contrast to Figure 5.3) that we have obtained when coating the water vapour 60 seconds after spreading the polymer layer onto the cooled water surface. Take note of the parallel orientation (in three directions) of the pores. For a better determination of the geometrical parameters, a few cells are shown in Figure 5.4b. It turns out that the cross section of the pore walls is plate shaped. The width of the pore walls is approximately 1.5 μm and the height of the "plate walls" about 0.25 μm. Inside the cell, one can perceive the breakthrough of the thin polymer film. Take note of the fact that the cross section of the pore walls of the latter structure does not have the shape of a T-section (in contrast to Figure 5.2).

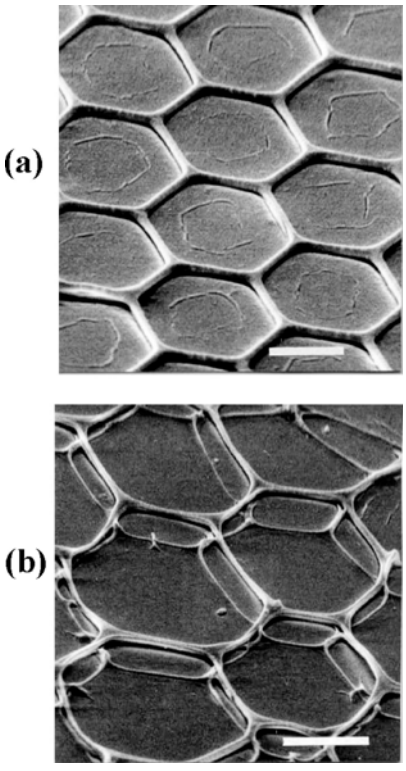

FIGURE 5.3. SEM images of different areas of one network with (a) a two-dimensional single cell and (b) a three-dimensional cell which was heated for 1 hour at a temperature of 950 °C under vacuum conditions. The network was prepared via coating the water vapour 10 seconds after having spread the polymer layer onto the cooled water surface. Scale bars: (a) 2 μm and (b) 4 μm.

5.3.2. Poly(p-Phenylenevinylene) and Poly(3-Octylthiophene) Networks

Figures 5.5 and 5.6 show SEM images of a fragment of the PPV precursor and polythiophene networks taken at different magnifications. The strong periodicity and homogeneity of the individual cells can be clearly recognized. For a closer look at the profile of the networks, atomic force microscopy (AFM) studies have been performed. The contact-mode topographic profiles of the PPV precursor network are displayed in Figure 5.7. The depth of the pores is 0.6 μm, the diameter about 1 μm and the width of the pore walls 0.7 μm. Corresponding values for conjugated polythiophene are 0.5 μm, 1.0 μm and 0.8 μm, respectively. Note that the pore wall of the PPV network is substantial in contrast to the polythiophene wall which is similar as the cellulose wall in Figure 5.4b. To end up with a conjugated PPV network, the sample of the PPV precursor network was annealed for 2 hours at a temperature of 160 °C under nitrogen flow atmosphere. The main finding is the following: the PPV precursor network converts to a conjugated PPV film that consists of periodic hill-like structures with a translational periodicity of the precursor network, i.e., the network melts to the film.

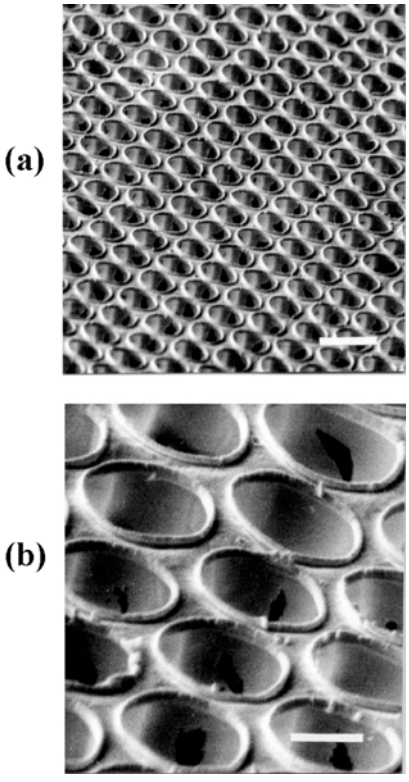

FIGURE 5.4. SEM images of a network with plate-shaped pore walls which were prepared via coating the water vapour 60 seconds after having spread the polymer layer onto the cooled water surface. Scale bars: (a) 5 μm and (b) 2 μm.

5.4. MODEL FOR THE FORMATION OF THE HONEYCOMB STRUCTURES IN POLYMER FILMS

When the fluid substance is placed at a liquid–air interface, it may spread out to thin film. It happens when a liquid of low surface tension is placed on one of a high surface tension. We have a positive spreading coefficient for all our polymer solutions in amyl acetate and in xylene. We have suggested that the size of thin xylene polymer solution layer on the water surface decreases with time. The latter can be explained as follows. In the experimental part, for the determination of the spreading coefficient $S_{F1/F2}$ (Equation (5.2)) we have used the surface tension values of the xylene solution, amyl acetate solution and water as for the pure liquids. However, when two liquids are in contact, they will become mutually saturated, so that $\sigma_{F2/G}$ will change to $\sigma_{F2(F1)/G}$, and $\sigma_{F1/G}$ to $\sigma_{F1(F2)/G}$. The symbol F1(F2) means that the liquid F1 is saturated with the liquid F2. The corresponding spreading coefficient has the symbol $S_{F1(F2)/F2(F1)}$ and can be determine as [18]

$$S_{F1(F2)/F2(F1)} = \sigma_{F2(F1)/G} - \sigma_{F1(F2)/G} - \sigma_{F1/F2}. \tag{5.3}$$

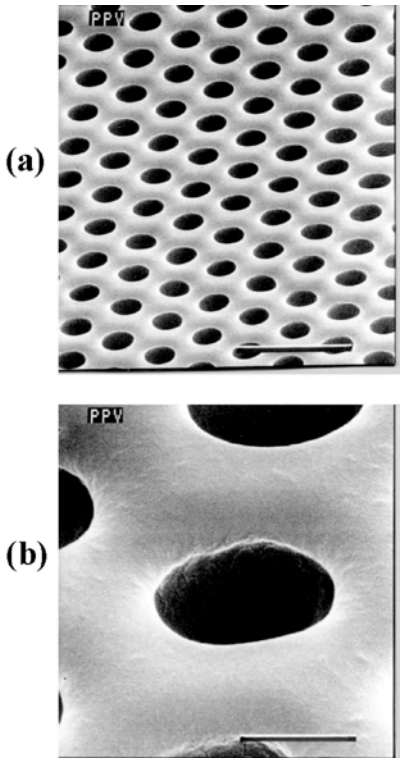

FIGURE 5.5. SEM images of a PPV precursor network. Scale bars: (a) 6 μm and (b) 1 μm.

In this case, for the solution of nitrocellulose in amyl acetate on the water surface (at 20 °C), we have $S_{F1(F2)/F2(F1)} = 39.5\,\text{mN/m} - 26.9\,\text{mN/m} - 12\,\text{mN/m} = 0.6\,\text{mN/m}$. The corresponding spreading coefficient for solutions of PPV (or P3OT) in xylene on the water surface is $S_{F1(F2)/F2(F1)} = 55.7\,\text{mN/m} - 28.8\,\text{mN/m} - 36.1\,\text{mN/m} = -9.2\,\text{mN/m}$, i.e., the final spreading coefficient is negative and the xylene polymer solution film retracts to a lens. This retraction is substantially smaller for the solution of nitrocellulose in amyl acetate. The values of the surface tension were determined using a stalagmometer. This instrument consists of a capillary tube through which the polymer solution flows, which enables the counting of the number of droplets and, therefore, the derivation of the surface tension.

Next, we look in a more detailed way at the lay on of the steam, because it represents one crucial factor for the patterning process. Since the cell diameter of our networks is about 2 μm, we investigate the shape of the water droplet with a diameter of 2 μm, before it dissolves on the surface of the polymer thin film. We have to compare two pressure quantities: the first one is the capillary pressure P_L which gives rise to the spherical shape of the droplet, the second one, the so-called gravitation pressure P_G, causes the flattening of the droplet. The capillary pressure can be calculated by the well-known formula $P_L = 2\sigma_{F2/G}/R$, with R giving the droplet radius. In our case, we obtain $P_L = 1.4 \times 10^9$ Pa. If the contact plane between the droplet and the polymer thin film

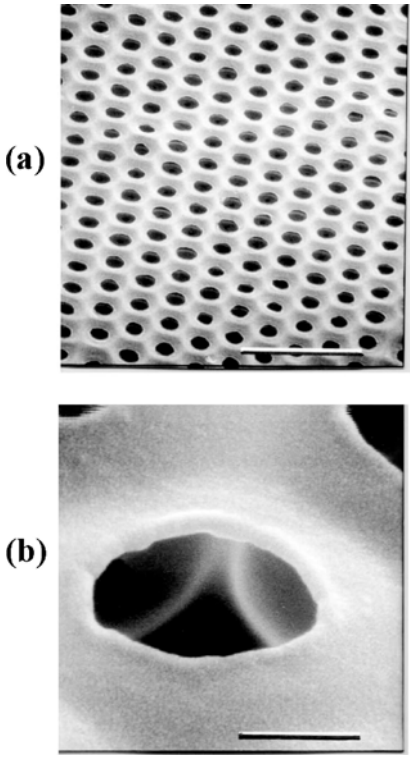

FIGURE 5.6. SEM images of a polythiophene network. Scale bars: (a) 6 μm and (b) 0.5 μm.

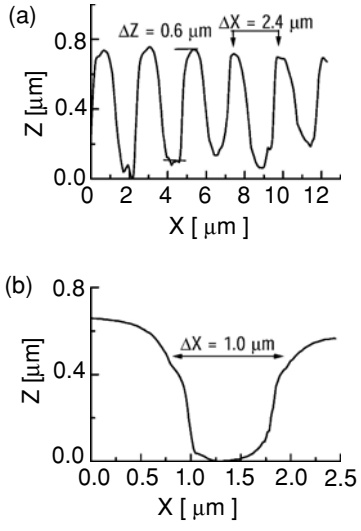

FIGURE 5.7. Contact-mode AFM images of the PPV precursor: (a) the profile of several pores to demonstrate the height distribution and (b) the profile of a single pore. *Z*: height; *X*: lateral coordinate.

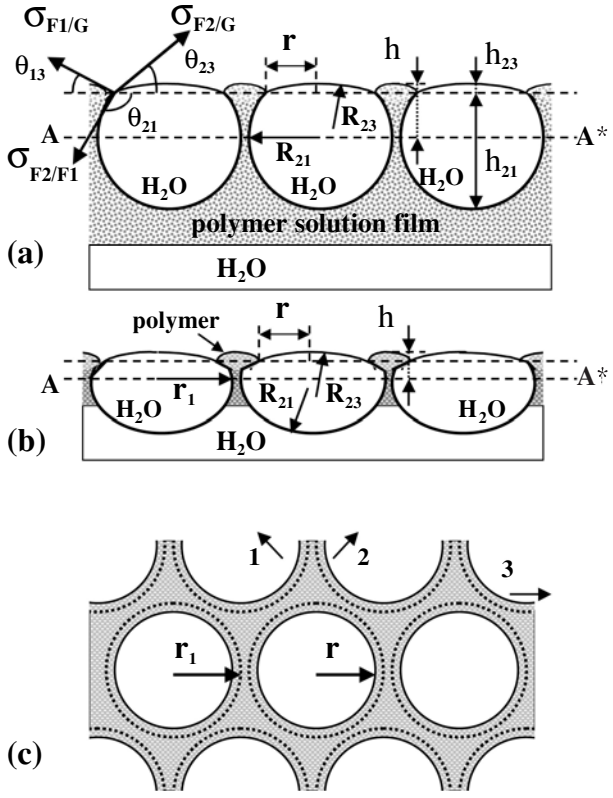

FIGURE 5.8. Model for the lay on of the water steam on the polymer layer: (a) process of envelopment of the water droplet by the polymer layer; the thin film on the surface of the water drop indicates a monomolecular polymer layer; (b) moment of the first contact of the water drop with the cooled water surface and (c) model structure of the network according to (b) in the plane of the polymer layer.

is approximately πR^2, we can determine $P_G = \text{mg}/\pi R^2$ with the water droplet mass $m = 4\pi R^3 \rho/3$ (ρ is the water density). Finally, one ends up with $P_G = 1.3 \times 10^{-2}$ Pa. If we compare both types of pressure, it is obviously $P_L \gg P_G$. This means that the water droplet has a spherical shape before laying on the surface of polymer solution. The first moment the water droplet contacts the polymer layer is sketched in Figure 5.8a: As the droplet touches the surface, its destruction will start. The angles θ_{21} and θ_{23}, in this case, are nonequalized boundary angles, because they experience variations in the development of further physical and chemical processes that take place at the phase boundary.

Water is a denser medium than amyl acetate (0.87 g/cm^3) and xylene (0.87 g/cm^3), but the water droplets do not sink because of a subtle balance between buoyancy, droplet weight and capillary forces [19]. The droplets are situated at the interface between the fluid polymer layer and air. Only a small part of the droplet is situated above the surface of the fluid polymer layer. The water droplets on the fluid polymer layer do not coalesce immediately when they touch because they are separated by a thin film of the polymer

solution. It is assumed that a thin polymer film (only a few monomolecular layers thick) is formed on the top of the droplets similar to the spreading of the polymer solution drop on the water surface. This thin film on the top of the water droplet might be the cause for stopping the growing of the water droplets and therefore a key parameter for the droplets size regulation. Additionally, we have suggested that water droplets in the polymer solution are covered with a solid polymer layer at the interface between the two liquids. Experimentally, this layer can be seen in Figures 5.4 and 5.6, which are characterized by the bursting holes (black); the water flows out of them after the solvent has evaporated. This layer prevented coalescence of water droplets, i.e., the precipitation of nitrocellulose, PPV and P3OT at the interface between the polymer solution and the water droplets is the basis for the formation of a compact hexagonal structure of water droplets. In our modelled Figure 5.8a, the precipitation layer is illustrated as a fat line between the water droplets and the polymer solution. Similar results were determined for the system of water droplets on the surface of solution of poly(*p*-phenylene)-block-polystyrene in carbon disulfide [12]. In Figure 5.8a, the corresponding forces which come into play at the above phase boundary are indicated. These forces converted to the length unit of the wetting line are equivalent to the corresponding quantities of the surface tension. From the condition that gives the balance of the surface tensions, the equilibrium state at the edge circumference of the contact between the water droplet and the polymer layer can be described by the following two equations

$$\sigma_{\mathrm{F1/G}} \cos \theta_{13} = \sigma_{\mathrm{F2/G}} \cos \theta_{23} + \sigma_{\mathrm{F2/F1}} \cos \theta_{21}, \tag{5.4}$$

$$\sigma_{\mathrm{F2/G}} \sin \theta_{23} + \sigma_{\mathrm{F1/G}} \sin \theta_{13} = \sigma_{\mathrm{F2/F1}} \sin \theta_{21}, \tag{5.5}$$

with the angles θ_{ij} as defined in Figure 5.8a. Equation (5.4) treats the balance of forces in the plane of the polymer layer and Equation (5.5) the balance of forces directed perpendicular to it.

For further qualitative discussion of the water droplet shape (the angles θ_{ij} in Figure 5.8a) only the initial values of surface tension σ had been used. The water droplet shape on the surface of paraffin oil had been studied by Knobler and Beysens [20] and on the surface of carbon disulfide by Pitois and Francois [12]. They have suggested that the water droplet has the form of a very asymmetric lens, the major part of which is nearly a complete sphere suspended from the surface. Based on these studies and from our experimental results in Figures 5.4–5.6, the shape of the water droplet on the surface of the polymer solution in xylene (or amyl acetate) has been sketched in Figure 5.8a. In our case, the capillary pressure in water droplet is drastically higher as the gravitation pressure ($P_{\mathrm{L}} \gg P_{\mathrm{G}}$), i.e., the influence of the gravity forces on the droplet shape can be neglected. This means that the small water droplet on the fluid polymer layer is composed of two spherical segments, whose angles θ_{ij} and radii R_{ij} can be determined by the surface tension forces [21]:

$$\cos \theta_{ij} = [1 + (\sigma_{ij}/\sigma_{jk})^2 - (\sigma_{ik}/\sigma_{jk})^2]/2(\sigma_{ij}/\sigma_{jk}), \tag{5.6}$$

$$R_{ij}/r = 1/\sin \theta_{\mathrm{ij}}, \tag{5.7}$$

$$h_{\mathrm{ij}}/r = (1 - \cos \theta_{ij})/\sin \theta_{ij}, \tag{5.8}$$

where θ_{ij}, R_{ij}, h_{ij} and r are defined as illustrated in Figure 5.8a. It should be noted that in this case, for an extremely small lens, Princen [21] has assumed that angle

θ_{13} in Figure 5.8a is zero. From Equation (5.6), for the water droplet on the surface of the polymer solution in xylene with $\sigma_{F1/G} = 30.0$ mN/m, $\sigma_{F2/F1} = 55.7$ mN/m and $\sigma_{F2/G} = 72.9$ mN/m, we have determined the angles which are $\theta_{21} = 113^\circ$ and $\theta_{23} = 45^\circ$. On the other hand, for the water droplet on the surface of paraffin oil, the angles θ_{ij} were measured by Knobler and Beysens [20]. From this study it follows that the values of the angles are $\theta_{13} = 135^\circ$–140°, $\theta_{23} = 20^\circ$–25°. The fluid properties (surface tension, density) of xylene and of paraffin oil are comparable. The force $\sigma_{F1/G} \sin \theta_{13} \times 2\pi R$ in Equation (5.5) does not permit that the water droplet sinks in the polymer solution layer, i.e., the angle θ_{13} cannot be 0. For the water droplet with a diameter of 2 μm in our case, the deflection of the force $\sigma_{F1/G}$ from a horizontal line is not very large and a experimental determination of the angle θ_{13} is not easy.

At the moment of the first contact between the water droplet and the fluid polymer layer the force $\sigma_{F2/G} \sin \theta_{23}$ for achieving the equilibrium state (described by Equation (5.5)) tends to pull the polymer layer onto the water droplet. The water droplet more and more penetrates the polymer layer. The envelopment of the water droplet by the polymer layer will take place as long as the angles θ_{21}, θ_{23} and θ_{13} (or the diameter of the surface curvatures, R_{21} and R_{23}, see Figure 5.8a) experience variations such that the pressure inside the water droplet caused by the surface curvature of the boundary water—air is equal to the pressure which results from the surface curvature at the boundary water—polymer layer. Their balance can be expressed mathematically by

$$\sigma_{F2/G}/R_{23} = \sigma_{F2/F1}/R_{21}, \tag{5.9}$$

where R_{23} and R_{21} are the radii of the water droplet at the boundary water—air and water—polymer layer, respectively. If we substitute the above values in Equation (5.9), we obtain the ratio $R_{23}/R_{21} \approx 1.3$ for the polymer solutions in xylene. This means that pressure equality in the lower and upper part of the water droplet at thermodynamical equilibrium can only be granted if R_{23} exceeds R_{21} by a factor 1.3 (see Figure 5.8a) for PPV (or P3OT) in xylene. On the other hand, a same value of the relation R_{23}/R_{21} can be determined from Equation (5.7), i.e., $R_{23}/R_{21} = \sin \theta_{21}/\sin \theta_{23} \approx 1.3$ with $\theta_{21} = 113^\circ$ and $\theta_{23} = 45^\circ$.

The formation of the hexagonally arranged layer of the water droplets on the liquid polymer layer can be explained as follows. With the water vapour condensation on the cold surface of the liquid, the water droplets form to a pattern of breath figures [22–25], for which the geometry can be very different. The physical basis of the breath figure formation on the fluid surfaces is discussed by Knobler and Beysens [20] and by Steyer *et al.* [26,9]. It is suggested that the formation of breath figures on fluid surfaces evolves through three stages: (a) initial stage, when droplets are isolated and do not interact strongly, and the average droplet radius $\langle R \rangle$ increases with time as $\langle R \rangle \propto t^{1/3}$; (b) crossover stage, when the surface coverage is high, and the rate of the droplet growth increases and (c) coalescence-dominated stage, when the surface coverage is high and constant, and the droplet radius increases as $\langle R \rangle \propto t$.

The attractive force F between two water droplets on the surface of the polymer solution separated by a distance l is determined by Chan *et al.* [19] and by Steyer *et al.* [9] as

$$F = (4\pi R^6 \rho^2 g^2 / 3l\sigma_{F1/G})[1/\rho_s + 0.25(1 - p^2)^{1.5} - 0.75(1 - p^2)^{0.5}]^2 \tag{5.10}$$

where R is the radius of the droplets, ρ is the absolute density of the polymer solution, g is the earth's gravitational acceleration, $\sigma_{F1/G}$ is the surface tension between the polymer solution and air, ρ_s is the relative density of the polymer solution to air and $p = r/R_{21}$, where r and R_{21} are radii illustrated in Figure 5.8a. This equation is valid when the bond number $B_0 = R^2\rho g/\sigma_{F1/G}$ is small enough (<0.1, see [19]). In our case, B_0 is of the order of 10^{-6} for all the polymer solutions and for the water droplets with a diameter of 2 μm. The parameter p characterizes the contact angles of the water droplet with the surface of the polymer solution and is very sensitive to the wetting properties between the water and the polymer solution. Steyer *et al.* [9] have suggested that the formation of the hexagonal structure of water droplets occurs when the parameter p has a value in the range from 0.4 to 0.8. The hexagonal structure disappears when p has a value in the range from 0.2 to 0.4.

In our case, the exact determination of parameter p and the corresponding force F is not easy, because initial values of the parameters $\sigma_{F2/G}$, $\sigma_{F1/G}$, $\sigma_{F2/F1}$ and ρ alter with time. In this case, it is of interest to consider only some tendency according to Equation (5.10) with initial values of the surface tension σ. From Equation (5.10) follows that by altering p the force can increase considerably, i.e., the value of p can be a key parameter for the formation of a hexagonal structure of water droplets. In our case, the value of the parameter p can be estimated from Equation (5.7). For the value of the angle $\theta_{21} = 113^\circ$, the calculated value is $p \approx 0.9$. The corresponding experimental value of p which follows from geometrical sizes of a single cell in Figures 5.2 and 5.5 is equal to 0.8 for a nitrocellulose network and 0.6 for a P3OT network. From Equation (5.8) follows that for $\theta_{23} = 45^\circ$ and $r \approx 0.9$ μm (for $R_{21} = 1$ μm) the value of the parameter $h_{23} \approx 0.4$ μm and for $\theta_{21} = 113^\circ$ the value of the parameter $h_{21} \approx 1.4$ μm.

On increasing $\sigma_{F1/G}$, the attractive force F between the two water droplets decreases and the corresponding distance l between droplets increases. We can see this fact in Figures 5.2 and 5.5. The width of the pore walls for the solutions of PPV in xylene (with $\sigma_{F1/G}$ (20 °C) = 30 mN/m) is 0.7 μm, and for a nitrocellulose solution in amyl acetate (with $\sigma_{F1/G}$ (20 °C) = 24.6 mN/m) the width is 0.25 μm. Turning to Figure 5.4, the corresponding nitrocellulose network which is obtained when coating the water vapour 60 seconds after spreading the polymer layer onto the cooled water surface has the width of the pore wall about 1.0 μm. This means that the surface tension of nitrocellulose solution increased (with solvent evaporation).

During the drying process of the polymer film, the water droplets approach the cooled water surface. In Figure 5.8b, the contact between the water droplet and the cooled water surface together with the corresponding variation in the radii R_{23} and R_{21} are displayed. Between the water droplet and the cooled water surface, we find a thin precipitation polymer film. The radius R_{21} will be enlarged, since the lower part of the water droplet which is in contact with the cooled water surface (more precisely, with the thin polymer film) will have a flat boundary plane. In Figure 5.8b, the cross section of the pore wall of one cell of the polymer network is shown which develops between two neighbouring water droplets. If we compare Figure 5.8b and Figure 5.2, we can recognize a pronounced similarity between the cross section of the experimentally prepared single cell of the polymer network and the one of the above modelled cell. From the figures, we conclude that the minimum thickness of the polymer layer in the middle of the frame (i.e., the base plate) corresponds to the minimum distance between

the water droplets near the AA* line. For nitrocellulose in amyl acetate, this distance is probably a few monomolecular layers thick, but for PPV in xylene this distance is about 0.7 μm. It should be noted that this distance difference between nitrocellulose and PPV can be explained first of all with the larger distance between condensed water droplets on the surface of the solution PPV in xylene. It follows from Equation (5.10) that increasing $\sigma_{F1/G}$ for PPV in xylene in comparison to nitrocellulose in amyl acetate leads to a smaller attractive force F between two water droplets and, accordingly, to a larger distance l between droplets. Second, it is possible that the precipitation of PPV at the solution–water interface is larger than that of nitrocellulose.

The appearance of small areas ($(30 \times 30)\ \mu m^2$) at the centre of the nitrocellulose network stripes (Figure 5.2, the single cell on the edge of stripe is of 2 μm), with basic cells as displayed in Figure 5.3b, results from some size gradient of the water vapour droplets. The formation of hexagonally arranged layer of water droplets on the liquid polymer layer with a size gradient of water droplets can be explained as follows. With the water vapour condensation on the cold surface of the liquid in the first moment, the water droplets conform the islands which build later the breath figures [22–25]. The islands attract each other in a much stronger way than the single droplets. This is because the attractive force F between the islands is proportional to the sixth power of their radii as in Equation (5.10). The intrinsic droplets in the stripe have the maximal shrinkage, and they can coalesce when a polymer film between the water droplets is not large enough. In the case of the water vapour with an extension comparable to the thickness of the polymer layer (4 μm), the total polymer solution will even move to the space in between the water droplets. As a consequence, there only remains a quite thin polymer film underneath the water droplets such that the polymer solution will be uniformly distributed with respect to the AA* line. The subsequent evaporation of amyl acetate out of the solution does not give rise to an essential redistribution of the polymer relating to the AA* line. We end up with the result that the cells shown in Figure 5.3b are, with respect to the third dimension, deeper (1.5 μm) than those shown in Figure 5.2 (0.5 μm). Moreover, they undergo a stronger symmetry with respect to the AA* line.

Figures 5.2, 5.4–5.6 and 5.8 give rise to the assumption that, first, the solidification of the polymer network (i.e., the evaporation of amyl acetate or xylene) takes place, and afterwards the water droplet will break through the thin polymer film and flow into the cooled water (compare the bursting holes (black) within the cells in Figures 5.4 and 5.6). As already noted above, the thickness of the liquid polymer layer is about 4 μm after dissolving on the water surface. During the drying process, the thickness of the polymer layer amounts to about 0.5 μm. As you can see in Figures 5.2 and 5.8, the whole polymer dissolved in amyl acetate (or xylene) is solidified in the AA* region, more precisely, above that line.

If the height h (Figure 5.8b) of the enveloping polymer layer is not too large, a hexagonal patterning can be achieved. The experimental realization is illustrated in Figures 5.2, 5.5 and 5.6. The underlying basic structure is outlined in Figure 5.8c. This means that, at a low height, the width of the pore wall will also be small. The junctions cross in the knots of the hexagonal network at the angle of 120° and usually form a continuous network. In Figure 5.8c, you can see that the hexagonal network developed at small values of h results in three types of zig-zag lines which proceed to the directions

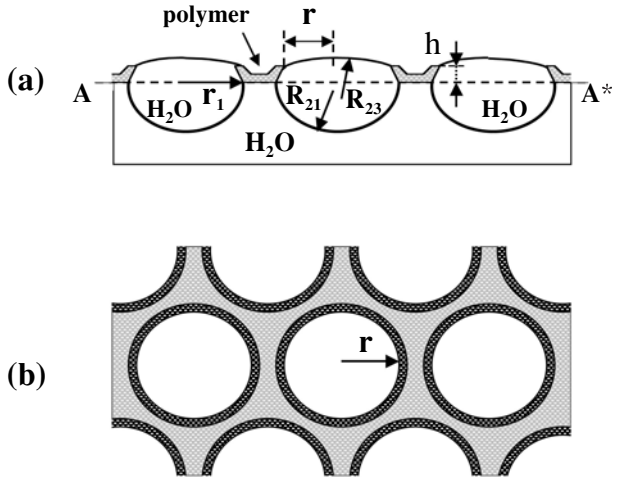

FIGURE 5.9. Model structure of the network according to the experimental situation in Figure 5.4. (a) Shape of the cross section of the pore wall and (b) form of the network. Parameter r_1 is the radius of the deformed water droplets.

1, 2, 3. It must be emphasized that the hexagonal shape of the single cells of the polymer network becomes clearer during evaporation.

In the case where the water vapour begins to affect the nitrocellulose layer not until 60 seconds after spreading it onto the cooled water surface, the thin polymer film gradually becomes dry in the meantime. In other words, the evaporation of amyl acetate out of the polymer layer during the elapsed time of 60 seconds gives rise to an increasing concentration of the polymer inside the polymer film. As a consequence, the distance between the neighbouring droplets of water vapour that precipitate onto the liquid surface of the polymer layer increases ($\sigma_{F1/G}$ is larger, Equation (5.10)). Accordingly, the same holds for the interspace between the neighbouring droplets of the water vapour where the polymer material accumulates after the polymer thin film has completely become dry (in the vicinity of the AA* line). In this case, the cross section of the pore wall will have the shape of a plate (Figure 5.9a), and the whole network resembles that one shown in Figure 5.9b. The lifted edges in Figure 5.9a are displayed together with the different pattern in Figure 5.9b. Upon comparing the experimental results in Figure 5.4 with the modelled networks in Figure 5.9, one recognizes a good correspondence.

5.5. APPLICATION OF POLYMER NETWORKS

5.5.1. Nitrocellulose Networks as Precursor for Carbon Networks

Carbon networks fabricated by the above-described method of a self-organized process represent porous disordered systems for electrical conductivity. The degree of disorder and, accordingly, the values of their electrical conductivity extending from insulator to metal behaviour change via heat treatment under vacuum conditions at process

temperatures in the range from 600 °C to 1000 °C. Upon varying the ambient temperature from 4.2 K to 295 K, four transport mechanisms can be observed [27,28]. For carbon networks (Figure 5.3a) whose conductivity is far beyond the metal–insulator transition (MIT), the specific resistivity ρ_c depends on the temperature T as $\rho_c(T) \propto T^{-b}$ exp $([T_0/T])^{1/m}$, where T_0 is a constant. In the low-temperature range, a Coulomb gap in the density of states located near the Fermi energy level occurs, that means, the characteristic value of the exponent is $m = 2$. At high temperatures, the pre-exponential part $\rho_c(T) \propto T^{-b}$ dominates. In the intermediate temperature range, Mott's hopping law with $m = 3$ follows. However, the specific resistivity of the carbon networks subject close to the MIT follows the power law $\rho_c(T) \propto T^{-b}$ with $0 \leq b \leq 3$ at low temperatures. In the high-temperature range, the specific resistivity is characterized by $\rho_c(T) \propto \exp(-[T/T_1]^{c-1})$, where the values for c are varying from 1.3 to 1.5 and T_1 is a constant. The above four charge transport mechanisms can be explained by the tails in the density of localized states pulled out of the conduction and valence band, as a consequence of disorder and in particular by some overlap between these tails.

The influence of the electrical field on the variable range hopping process of porous carbon networks is examined in the range of the validity of the law $\ln \sigma_c(T) \propto -(T_0/T)^{1/2}$ (Coulomb gap), where σ_c means electrical conductivity. It is shown that the field dependence of the samples investigated in the vicinity of the metal–insulator transition clearly distinguishes four characteristic regions [29]. At low values of the electrical field applied, we have ohmic conductivity. Upon increasing the electrical field E, the electrical conductivity σ_c rises, first following the law $\ln \sigma_c(E) \propto E^n$, where n changes from 1.4 to 2.6 with increasing distance from the metal–insulator transition on the insulating side. Then, at higher electrical field, the conductivity turns to the relation $\ln \sigma_c(E) \propto E^{1.0}$. The temperature dependence of the hopping length l_h of the charge carriers, determined within the above field regime, develops as $l_h(T) \propto T^{-0.9}$. At temperatures where the ohmic behaviour in the Coulomb gap occurs and obeys the law $\ln \sigma_c(T) \propto -(T_0/T)^{1/2}$, the electrical conductivity caused by thermally nonactivated charge carriers at high fields complies with $\ln \sigma_c(E) \propto E^{-1/3}$. The current density j changes as $\ln j(E) \propto E^{-1/6}$. The temperature dependence of the threshold electrical field E_{th}, which characterizes the transition from the low-field to the high-field range, follows $E_{th} \propto T^{1.5}$.

5.5.2. Nitrocellulose Network as Mask for Ion-Etching Process

The nitrocellulose network is placed on a GaAs epitaxial layer with an area of (240 × 330) μm^2, a thickness of 0.25 μm and an electron concentration of $1.3 \times 10^{17} cm^{-3}$ (Figure 5.10a). On this layer, GeAu contacts ensure ohmic contacts. The network represents a mask for the following Ar-ion-etching process with an energy of 3.5 keV. Due the difference in the etching velocity between cellulose and GaAs, the cellulose mask was totally removed in a time span of 90 seconds. Also, the GaAs layer is removed in the meshes of the cellulose network, and the network structure is transferred to the GaAs layer (Figure 5.10b). The diameter of the hexagonal meshes is about 1 μm, and the width of the walls extends from 50 nm to 100 nm. The etching process was controlled by the use of Auger spectroscopy.

The transport properties of patterned GaAs exhibit interesting phenomena [30]. In a wide low-temperature regime up to 260 K, we find variable range hopping in two

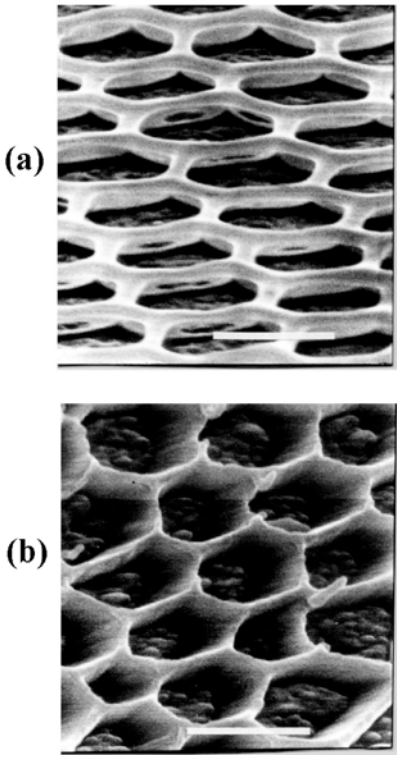

FIGURE 5.10. SEM images of (a) a nitrocellulose mask and (b) a GaAs network obtained by an ion-etching process. Scale bars: (a) 0.6 μm and (b) 0.75 μm.

dimensions with a nearly constant density of states of the defect band. The absolute values obtained by an adaptation of the local activation energy to predictions of theory are in good agreement with those reported in literature on thin bulk material. We have also analyzed the nonlinear voltage dependence of the differential conductivity by percolation theory. The onset of nonlinearity can be described by a threshold, i.e., a critical current. Between the local activation energy and the critical current, a good correlation of the different temperature regimes is found for which a transport mechanism is valid.

5.6. CONCLUSION

An experimental preparation technique was described that is capable to produce mesoscopic polymer network structures with different shapes of the basic cell: A drop of the initial polymer solution spreads onto a cooled water surface, and the water vapour interacts with the resulting polymer thin film. Following the self-organization process of precipitating droplets of the water vapour on the polymer layer, pulling the latter to the water droplets, and subsequently evaporating the solvent, the originally homogeneous polymer film proceeds to a hexagonal network pattern. It was demonstrated that the size

of the basic hexagonal cell is determined by the diameter of the water vapour droplets used during preparation. It was suggested that the stabilization of water droplets on the fluid surface is indispensable for ordered structure formation. This is performed by the ability of the polymer to precipitate at the solution–water interface. The properties of different polymer solutions are discussed that can influence a growth rate, a size and a form of condensing water droplets, and their interaction between each other. By the help of an elementary model study on the self-organized structuring process in the liquid polymer films, it was succeeded in specifying and interpreting the morphology of the basic network cells observed experimentally.

ACKNOWLEDGMENTS

I acknowledge with much thanks my colleague I. Bashmakov for successful cooperation and fruitful discussions. I would like to thank G. H. Bauer and J. Parisi for very helpful discussions, and moreover to V. Uchov and S. Martyna for taking the scanning electron microscopy pictures.

REFERENCES

[1] R.R. Bhave, *Inorganic Membranes: Synthesis, Characteristics and Applications*, Van Nostrand Reinhold, New York, 1991.
[2] E. Yablonovitch, Inhibited spontaneous emission in solid-state physics and electronics, Phys. Rev. Lett. **58**(20), 2059–2062 (1987).
[3] N. Akoezbek and S. John, Optical solitary waves in two- and three-dimensional nonlinear photonic band-gap structures, Phys. Rev. E. **57**(2), 2287–2319 (1998).
[4] K. Busch and S. John, Photonic band gap formation in certain self-organizing systems, Phys. Rev. E **58**(3), 3896–3908 (1998).
[5] T. Bitzer, *Honeycomb Technology*, Chapman and Hall, London, 1997.
[6] S.A. Jenekhe and X.L. Chen, Self-assembly of ordered microporous material from rod–coil block copolymers, Science **283**, 372–375 (1999).
[7] Y. Xia, B. Gates, Y. Yin and Y. Lu, Monodispersed colloidal spheres: old materials with new applications, Adv. Mater. **12**(10), 693–713 (2000).
[8] D.J. Norris and Yu, A. Vlasov, Chemical approaches to three-dimensional semiconductor photonic crystals, Adv. Mater. **13**(6), 371–376 (2000).
[9] A. Steyer, P. Guenoun and D. Beysens, Hexatic and fat-fractal structures for water droplets condensing on oil, Phys. Rev. E. **48**(1), 428–431 (1993).
[10] G. Widawski, M. Rawiso and B. Francois, Self-organized honeycomb morphology of star-polymer polystyrene films, Nature **369**, 387–389 (1994).
[11] B. Francois, O. Pitois and J. Francois, Polymer films with a self-organized honeycomb morphology, Adv. Mater. **7**(12), 1041–1044 (1995).
[12] O. Pitois and B. Francois, Formation of ordered micro-porous membranes, Eur. Phys. J. B **8**, 225–231 (1999).
[13] O. Karthaus, N. Maruyama, X. Cieren, M. Shimomura, H. Hasegawa and T. Hashimoto, Water-assisted formation of micrometer-size honeycomb patterns of polymers, Langmuir **16**(15), 6071–6076 (2000).
[14] M. Srinivasarao, D. Collings, A. Philips and S. Patel, Three-dimensionally ordered array of air bubbles in a polymer film, Science **292**, 79–83 (2001).
[15] L.V. Govor, I.B. Butylina, I.A. Bashmakov, I.M. Grigorieva, V.K. Ksenevich and V.A. Samuilov, in *Advanced Semiconductor Devices and Microsystems*, Ed. T. Labinsky, Smolenice, Slovakia, 1996, pp. 81–83.

[16] L.V. Govor, I.A. Bashmakov, F.N. Kaputski, M. Pientka and J. Parisi, Self-organized formation of low-dimensional network structures starting from a nitrocellulose solution, Macromol. Chem. Phys. **201**(18), 2721–2728 (2000).
[17] L.V. Govor, I.A. Bashmakov, R. Kiebooms, V. Dyakonov and J. Parisi, Self-organized networks based on conjugated polymers, Adv. Mater. **13**(8), 588–591 (2001).
[18] A.W. Adamson, *Physical Chemistry of Surfaces*, Wiley, New York, 1982.
[19] D.Y.C. Chan, J.D. Henry and L.R. White, The interaction of colloidal particles collected at fluid interface, J. Colloid Interface Sci. **79**(2), 410–418 (1981).
[20] C.M. Knobler and D. Beysens, Growth of breath figures on fluid surfaces, Europhys. Lett. **6**(8), 707–712 (1988).
[21] H.M. Princen, in *Surface and Colloid Science*, Ed. E. Matijevic,Vol. 2, Wiley-Interscience, New York, 1969, pp. 1–84.
[22] D. Beysens and C.M. Knobler, Growth of breath figures, Phys. Rev. Lett. **57**(12), 1433–1436 (1986).
[23] F. Family and P. Meakin, Scaling of the droplet-size distribution in vapor-deposited thin films, Phys. Rev. Lett. **61**(4), 428–431 (1988).
[24] B.J. Briscoe and K.P. Galvin, The evolution of a 2D constrained growth system of droplets-breath figures, J. Phys. D: Appl. Phys. **23**(4), 422–428 (1990).
[25] A.V. Limaye, R.D. Narhe, A.M. Dhote and S.B. Ogale, Evidence for convective effects in breath figure formation on volatile fluid surfaces, Phys. Rev. Lett. **79**(20), 3762–3765 (1996).
[26] A. Steyer, P. Guenoun and D. Beysens, Two-dimensional ordering during droplet growth on a liquid surface, Phys. Rev. B **42**(1), 1086–1089 (1990).
[27] L.V. Govor, M. Goldbach, I.A. Bashmakov, I.B. Butylina and J. Parisi, Electrical properties of self-assembled carbon networks, Phys. Rev. B **62**(3), 2201–2208 (2000).
[28] L.V. Govor, I.A. Bashmakov, K. Boehme, M. Pientka and J. Parisi, Coulomb gap and variable-range hopping in self-organized carbon networks, J. Appl. Phys. **90**(3), 1307–1313 (2001).
[29] L.V. Govor, I.A. Bashmakov, K. Boehme and J. Parisi, Electrical field dependence of hopping conduction in self-organized carbon networks, J. Appl. Phys. **91**(2), 739–747 (2002).
[30] L.V. Govor, M. Goldbach, I.A. Bashmakov and J. Parisi, Preparation and electrical characterization of low-dimensional net structures made out of GaAs epitaxial layers, Phys. Lett. A **261**, 197–204 (1999).